

PIOTR STĘPIEŃ*

UNDEFORMED CHIP SIZES IN GRINDING PROCESS OF REGULAR SURFACE TEXTURE GENERATION

The paper presents theoretical analysis and simulation results of the process of regular surface texture generation by grinding with the wheel shaped in a special way. Simple variant of the method consists in grinding with the wheel having single helical groove. Non-uniform load of abrasive grains located in different zones of the wheel circumference was described. Two models (deterministic and probabilistic) of the wheel active surface were developed, assuming different grain arrangement. Results of two models were compared and differences were explained.

LIST OF SYMBOLS

- A_L – longitudinal cross-section area of undeformed chip,
- a_m – mean thickness of undeformed chip,
- a_{max} – maximal thickness of undeformed chip,
- b – bottom length of groove shaped on work-material,
- C_A – mean number of grains vertices per wheel surface unit,
- d – grinding depth,
- f_d – dressing feed equal to helical groove pitch,
- h – depth of helical groove,
- H – wheel height,
- l – length of undeformed chip,
- L – longitudinal pitch of grooves shaped on work-material,
- l_b – length of bearing segment on the work-material,
- l_c – length of wheel-work-material contact zone,
- l_g – mean distance between adjacent grain vertices,
- \bar{l}_g – mean directional distance between adjacent grain vertices,

* Department of Mechanical Engineering, Technical University of Koszalin, Raławicka 15-17, 75-620 Koszalin, Poland; E-mail: piotr.stepien@tu.koszalin.pl

-
- l_r – length of groove shaped on work-material,
 m – shape parameter of Weibull distribution,
 n – number of grain vertices at wheel circumference,
 n_A – number of active grain vertices at wheel circumference,
 n_{PA} – number of potential active grain vertices at wheel circumference,
 R – radius of grinding wheel,
 r – radius of imaginable wheel rolling without any slip along rolling line,
 r_D – radius of tip of tool used for shaping helical groove on the wheel,
 u – scale parameter of Weibull distribution,
 v^* – ratio between work feed and grinding speed,
 v_s – grinding speed,
 v_w – work-material feed,
 x_{en} – abscissa of point where grain enter into work-material,
 x_{ex} – abscissa of point where grain exit from work-material,
 α – angular coordinate of grain vertices in polar system,
 δH – elementary wheel slice width,
 $\Delta\alpha$ – angle between adjacent grain vertices in the plane perpendicular to wheel axis,
 $\Delta\rho$ – radial distance between grain vertices and nominal profile of grinding wheel,
 $\rho(\alpha)$ – radius of nominal profile of grinding wheel,
 φ – angle of grinding wheel rotation.

1. Introduction

Growing interest in machine elements having regular surface texture (RST), is manifested by: improving methods of surface measurement and description [1], [2], developing new methods of RST generation as well as new areas of application. Most of the methods of regular surface texture (RST) generation consist in shaping the set of regular grooves-cavities arranged in a regular way. Such surfaces show many advantageous features, regarding mainly tribological effects. The main features of RST are: reduction of fluid and boundary friction coefficients, absorbing of small hard particles from lubricant, reduction of residual stress and shape deviation, better damping capacity, better leak-tightness of static and dynamic couplings [3], [4], [5], [6], [7], [8], [9], [10], and better adherence of coating and adhesive bonds. In special applications RST provides decorative effects as well. RST may be generated by several methods, such as: precise diamond turning [11], rolling [12], embossing [9], [13], etching [4], [15], vibrorolling [5], [16], abrasive jet machining [17] and EDM [7], [18]. Impressive results of laser surface

texturing were presented in many recent papers [6], [8], [19], [20], [21], [22], [23], [24], [25], [26].

The method of RST generation by grinding with the specially shaped wheel was developed in 1988 [27] and presented in many papers [3], [10], [28], [29], [30], [31], [32], [33], [34], [35]. Practical application of the method for shaping ceramic discs of gas-lubricated and self acting thrust bearings was also presented [4], [36]. The presented method is a simple, inexpensive and productive alternative to better known methods of RST generation.

By shaping deep helical grooves on the wheel active surface, it is possible to obtain RST of the work-material surface by grinding. The result of the grinding process shows grooves-cavities of repeatable shape, arranged in a regular way. Such grinding does not change nominal dimension of work-material, and is a typical surface treatment machining. Pictorial scheme of the wheel circumference reproduction on the work-material is shown in Fig. 1 for two variants of the method. In both cases, the depth h of helical grooves must be greater than grinding depth d . The ratio $v^* = v_w/v_s$ should be great enough to ensure separation of individual grooves and adequate bearing area rested on the surface between grooves.

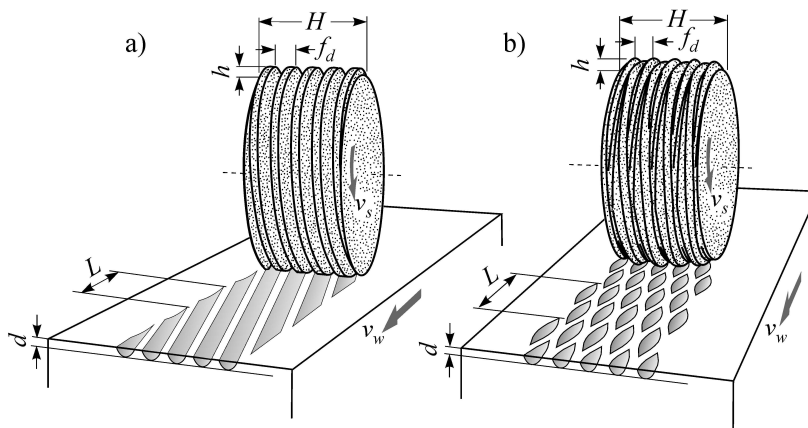


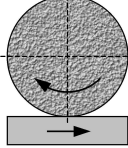
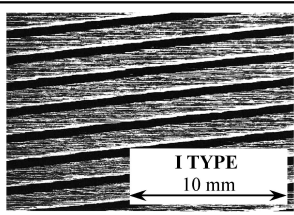
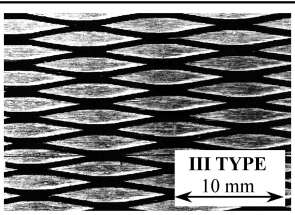
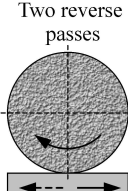
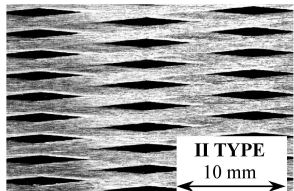
Fig. 1. Pictorial views of grinding with the wheels having single (a) and double (b) helical grooves for shaping regular pattern on a flat surface [10]

The method needs specially shaped grinding wheels. For shaping of helical grooves on conventional wheels with vitrified bond, the single point diamond dressers are usually applied. Diamond wheels with resinous bond may be shaped with SiC wheels [4], while super-hard, metal-bonded wheels may be shaped by EDM [37], [38].

The effect of excessive dressing feed (f_d) on ground surface topography had been described [39], [40], [41], [42], [43] as a grinding fault, generally. However, it is possible to generate RST by controlled grinding process with

the wheel shaped in a special way. Examples of three basic types of RST obtained with this method are given in Table 1.

Table 1. Three types of the grooved surface (top view photographs) obtained with the wheels having helical grooves – darker areas represent fragments of flat bearing surface [35]

GRINDING	WHEEL SHAPE	
	Single helical groove	Two helical grooves
One single pass 		
Two reverse passes 		Irregular surface texture

Untypical wheel shape and special performance of grinding process ($d < h$; high value of $v^* = v_w/v_s$ ratio) cause that the wheel work differs from conventional grinding. The main difference consists in non-uniform load of abrasive grains, caused by non-uniform distribution of undeformed chip sizes. By determining the sizes of undeformed chips, it is possible to develop models of grinding force and hence to predict wheel wear. Most of the questions concerning non-uniform load of grains may be explained by analysis of the simplest variant of grinding with the wheel having single helical groove.

2. Profile of the wheel with single helical groove

For general description, it was assumed that the profile of dresser tip is given by the function $y = f(z)$, as shown in Fig. 2a for the axial cross-section. Function $y = f(z)$ determines helical groove depth h , dressing feed f_d , length c of cylindrical fragment of wheel profile and angles κ_1 and κ_2 between the tangents to a helical groove profile and the wheel nominal surface. Simple conversion $z \rightarrow \alpha$ allows us to determine the wheel local radius $\rho(\alpha)$ for $0 \leq \alpha \leq 2\pi$, according to Eq. (1).

$$\rho(\alpha) = R - f\left(f_d \frac{\alpha}{2\pi}\right) \quad (1)$$

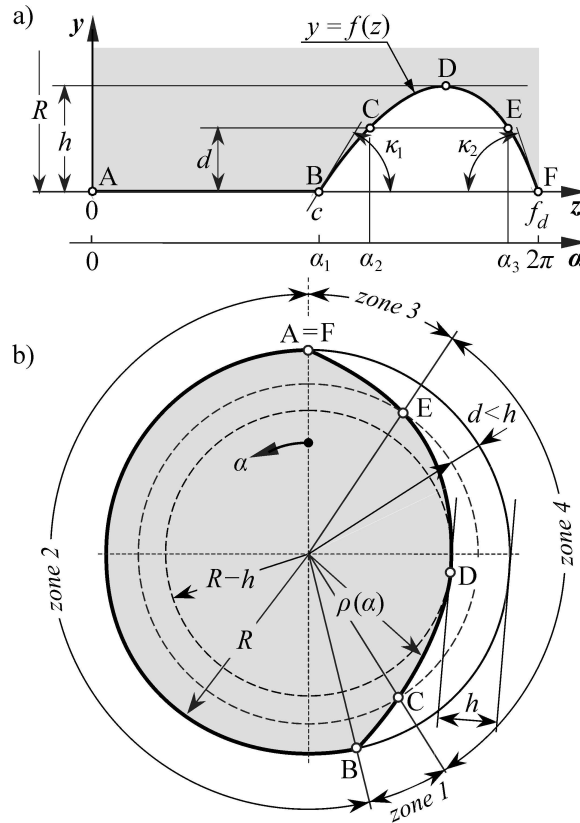


Fig. 2. Generalized axial cross-section (a) of the wheel and cross-section (b) in the plane perpendicular to wheel axis

Wheel local radius $\rho(\alpha)$ is diversified in the plane perpendicular to wheel axis, as it is shown in Fig. 2b with points denoted in the same way as in Fig. 2a. The polar system of coordinates $\rho(\alpha)$ assumes anticlockwise sense of angle α (Fig. 2b). Knowing the grinding depth d , one can indicate two points C and E, which limit the fragment of potential active wheel circumference. The entire wheel circumference is divided into four zones by characteristic points A, B, C, E of the wheel profile.

To obtain an adequate $c : f_d$ ratio (Fig. 2a), it is recommended to use diamond dresser with flat or rounded tips, for instance the worn ones. It is then possible to shape helical grooves with a big dressing feed f_d and small depth h , which reduces dressing force and wheel radius decrement

in successive wheel shaping. Assuming spherical shape of diamond dresser given by r_D radius, one can calculate the local wheel radius as:

$$\begin{cases} \rho(\alpha) = R & \text{for } 0 \leq \alpha < \alpha_1 \\ \rho(\alpha) = R - \sqrt{r_D^2 - \left(\alpha \frac{f_d}{2\pi} - \frac{f_d + c}{2}\right)^2} - r_D + h & \text{for } \alpha_1 \leq \alpha < 2\pi \end{cases} \quad (2)$$

Characteristic angles of wheel profile (Fig. 2a), which determine the sizes of the wheel cross-section zones (Fig. 2b), are then calculated by the following formulas:

$$\alpha_1 = 2\pi \left(1 - \frac{2\sqrt{h(2r_D - h)}}{f_d} \right) \quad (3a)$$

$$\alpha_2 = 2\pi \left(1 - \frac{\sqrt{h(2r_D - h)} + \sqrt{(h-d)(2r_D - h + d)}}{f_d} \right) \quad (3b)$$

$$\alpha_3 = 2\pi \left(1 - \frac{\sqrt{h(2r_D - h)} - \sqrt{(h-d)(2r_D - h + d)}}{f_d} \right) \quad (3c)$$

Angles $\kappa_1 = \kappa_2 = \kappa$ are equal to:

$$\text{tg}\kappa = \sqrt{\left(\frac{r_D}{r_D - h}\right)^2 - 1} \quad (4)$$

3. Paths of abrasive grains

It was assumed that the wheel rotates anticlockwise and wheel rotational position is defined by angle φ having the same sense as the angle α . Any point (vertex of abrasive grain) of the wheel circumference moves over a cycloid path. Paths of motion, relative to flat work-material, were developed for each grain in the coordinate systems shown in Fig. 3. An important parameter of the grinding kinematics is the radius $r = R(v_w/v_s) = Rv^*$ of imaginable wheel rolling without any slip along imaginable line.

The set of equations, for two kinematical variants of grinding, in the system OXY, connected with the centre of grinding wheel, is as follows:

$$\begin{array}{ll} \textit{for up-grinding:} & \textit{for down-grinding:} \\ \left\{ \begin{array}{l} X = r\varphi - \rho(\alpha) \sin(\alpha + \varphi) \\ Y = -\rho(\alpha) \cos(\alpha + \varphi) \end{array} \right. & \left\{ \begin{array}{l} X = r\varphi - \rho(\alpha) \sin(\alpha + \varphi) \\ Y = \rho(\alpha) \cos(\alpha + \varphi) \end{array} \right. \quad (5a, b) \end{array}$$

For attainable parameters (R, v_s, v_w), cycloid curvatures differ in a minimal degree for up- and down-grinding paths, and in Fig. 3 these differences are exaggerated.

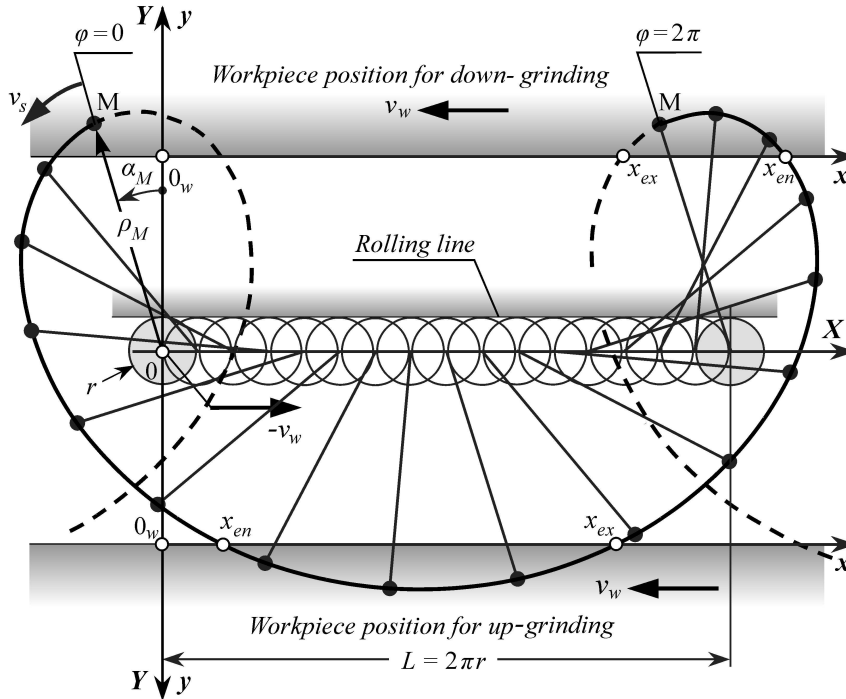


Fig. 3. Cycloid path of vertex M of abrasive grain, in position determined by polar coordinates $\rho_M(\alpha_M)$, during one full wheel rotation ($0 \leq \varphi \leq 2\pi$) for up- and down-grinding

Cycloids (5) were transformed by simple translation: $x = X$; $y = Y + d - R$ to coordinate system 0_wxy , connected with the nominal surface of work-material:

$$\left\{ \begin{array}{l} \text{for up-grinding:} \\ x = r\varphi - \rho(\alpha) \sin(\alpha + \varphi) \\ y = -\rho(\alpha) \cos(\alpha + \varphi) + g - R \end{array} \right. \quad \left\{ \begin{array}{l} \text{for down-grinding:} \\ x = r\varphi - \rho(\alpha) \sin(\alpha + \varphi) \\ y = \rho(\alpha) \cos(\alpha + \varphi) + g - R \end{array} \right. \quad (6a, b)$$

Each vertex of potential active grain, located at the radius $\rho(\alpha) \geq R - d$, (zones 1., 2. and 3.), enters work-material at the angle φ_{en} and leaves it at the angle φ_{ex} . Angles φ_{en} and φ_{ex} of wheel rotation can be calculated by substitution $y = 0$ in Eq. (6) and maintaining $\varphi_{en} < \varphi_{ex}$ condition. It makes it possible to determine abscissas x_{en} and x_{ex} of entrance and exit points:

$$\begin{array}{l}
 \text{for up-grinding:} \\
 \left. \begin{array}{l}
 \varphi_{en} = \arccos \left[\frac{d-R}{\rho(\alpha)} \right] - \alpha \\
 \varphi_{ex} = 2\pi - \arccos \left[\frac{d-R}{\rho(\alpha)} \right] - \alpha \\
 x_{en} = r\varphi_{en} - \rho(\alpha) \sin(\alpha + \varphi_{en})
 \end{array} \right\}
 \end{array}
 \quad
 \begin{array}{l}
 \text{for down-grinding:} \\
 \left. \begin{array}{l}
 \varphi_{en} = -\arccos \left[\frac{R-d}{\rho(\alpha)} \right] - \alpha \\
 \varphi_{ex} = \arccos \left[\frac{R-d}{\rho(\alpha)} \right] - \alpha \\
 x_{ex} = r\varphi_{ex} - \rho(\alpha) \sin(\alpha + \varphi_{ex})
 \end{array} \right\}
 \end{array}
 \quad (7a, b)$$

4. Undeformed chip sizes – deterministic model

Deterministic model of the wheel assumes that the wheel circumference, with helical groove shaped by dresser tip with circular profile, contains n vertices of abrasive grains, located exactly at radiuses $\rho(\alpha)$, given by Eq. (2). It is also assumed that grain vertices are arranged uniformly. It means that the angle $\Delta\alpha = 2\pi/n$ between adjacent vertices is equal and circumferential distance is given as $l_g \approx 2\pi R/n$. Such assumptions justify the model as deterministic one. Arrangement of abrasive grains is determined by following unique parameters: R , r_D , h , f_d , l_g , and the example of the model is shown in Fig. 4. Relative grain paths were calculated according to Eq. (6a) (up-grinding) for the wheel shaped as in Fig. 4, for each of $n = 90$ points, uniformly distributed along wheel circumference.

Figure 5 shows cycloids limited to their active fragments ($y \geq 0$; $x_{en} \leq x \leq x_{ex}$), for three different work feeds v_w . Grains located in zone 1 (Fig. 4) work in **indentation phase**, deepening the initial groove on work-material. The first grain in this phase (point C in Fig. 4) starts cutting at minimal depth, while last grain, located in point B (Fig. 4), shapes the left-side slope of the groove as the cycloid. The grains located in zone 2 work in **main phase** in the same way as for conventional up-grinding – they do not deepen the groove, enlarging it in the work feed direction. The last grain in this phase, located in point A (Fig. 4), shapes the right-side groove slope as the same cycloid, hence the groove profile becomes symmetrical. The grains located in zone 3 do not contact the work-material, and they pass over the groove surface shaped by the grains in main phase. This is the **exit phase**. Large fragment of the wheel circumference (zone 4) works in the so-called **idle phase** – grains can not contact the work-material because of $\rho(\alpha) < R - d$. In this phase, the work-material passes for some distance leaving a part of flat bearing surface. Paths of grains located in zone 1, for the next wheel rotation, are shown in Figs. 5a, b, c as the next sets of coarse black lines.

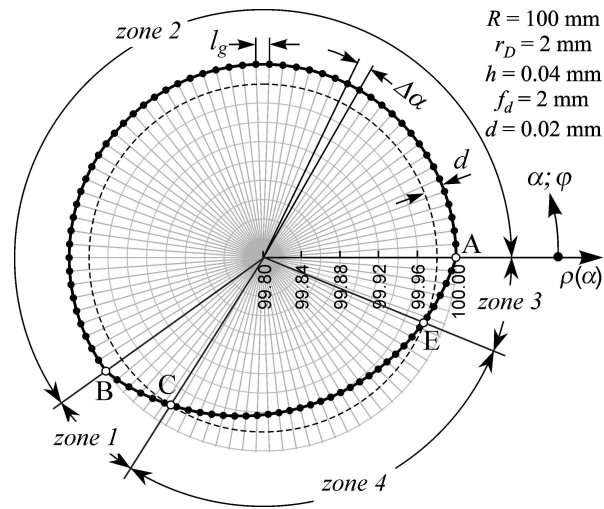


Fig. 4. Deterministic arrangement of grain vertices on circumference of wheel with helical groove

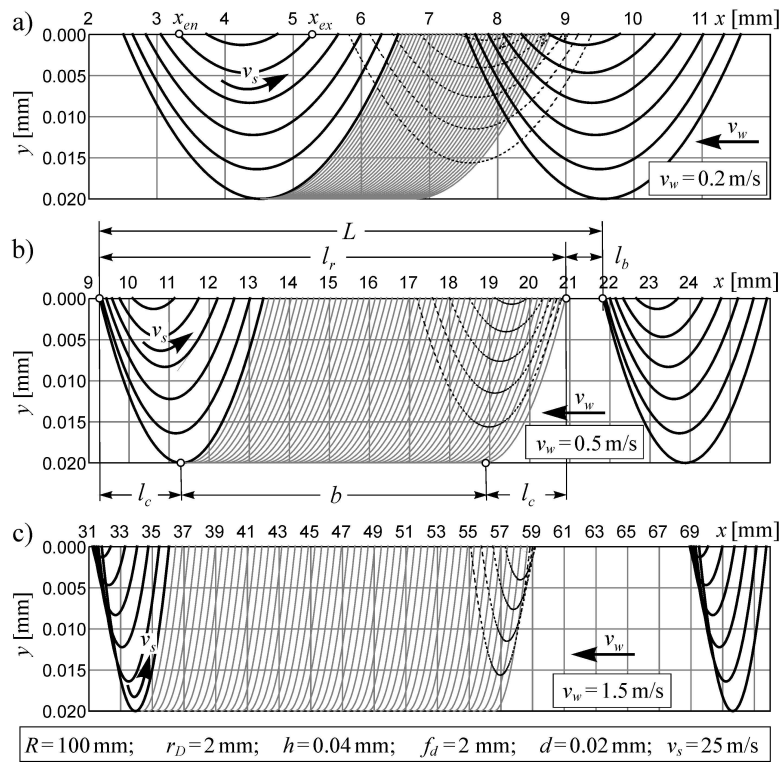


Fig. 5. Cycloid paths of grain vertices (up-grinding), located in zone 1 (coarse black lines), zone 2 (fine grey lines) and zone 3 (dashed lines) for the same wheel working with three different work feeds v_w

As it was mentioned in the first section, the ratio $v^* = v_w/v_s$ should reach an adequate value. If v^* is too small (smaller than lower critical value v_L^*), grooves shaped on the work surfaces are not separated from each other (Fig. 5a). Nominal dimension of work-material is reduced and no flat bearing fragments remain on the work-material. On the other hand, if v^* is too high (higher than upper critical value v_U^*), the slopes of the grooves shaped on the work-material are formed as the envelope of many cycloids. Such a case (Fig. 5c) is not a technological error, but needs more complicated description. In practice, work feed v_w is limited to the values, which fulfil the constrains $v_L^* < v^* < v_U^*$, and the result of it is shown in Fig. 5b. Grooves of length l_r and depth d shaped on the work-material are the result of wheel reproduction. Each groove consists of flat bottom (length b) and two curvilinear slopes (length l_c). The basic dimensions of the longitudinal groove profile are as follows:

$$\text{longitudinal pitch: } L = 2\pi Rv^*; \quad (8)$$

$$\text{bottom length: } b = 2\pi Rv^* \frac{l}{f_d} \quad (9)$$

$$\text{slope length: } l_{cUG} = \sqrt{2Rd - d^2}(1+v^*); \quad l_{cDG} = \sqrt{2Rd - d^2}(1 - v^*) \quad (10a, b)$$

The length of the groove $l_r = b + 2l_c$ and the length of bearing segment $l_b = L - l_r$ can be easily found as the resultant dimensions.

Adequate parameters should ensure longitudinal pitch of grooves L , greater than the groove length l_r , and nonzero segments l_b of bearing area should remain on the surface between grooves. The constraint ($L > l_r$) was used for determination of lower critical value v_L^* . The upper critical value v_U^* was determined from the constraint $\delta x_{en}/\delta \alpha > 0$. Further analysis of deterministic model was carried out for the cases fulfilling conditions (11) and (12), determined [10] for up- and down grinding, respectively:

$$v_L^* = \frac{\sqrt{2Rd - d^2}}{\pi R \left(1 - \frac{l}{f_d}\right) - \sqrt{2Rd - d^2}} < v^* < v_U^* = \left\{ \frac{2\pi \sqrt{2Rd - d^2}}{f_d \text{tg}[\min(|\kappa_1|; |\kappa_2|)]} - 1 \right\}^{-1} \quad (11a, b)$$

$$v_L^* = \frac{\sqrt{2Rd - d^2}}{\pi R \left(1 - \frac{l}{f_d}\right) + \sqrt{2Rd - d^2}} < v^* < v_U^* = \left\{ \frac{2\pi \sqrt{2Rd - d^2}}{f_d \text{tg}[\min(|\kappa_1|; |\kappa_2|)]} + 1 \right\}^{-1} \quad (12a, b)$$

Figure 5b shows that only grains located in zones 1 and 2 take part in the cutting process. Undeformed chips, cut by grains from zone 1, have different sizes, depending on grain location and radius $\rho(\alpha)$, while undeformed chips, cut by grains from zone 2, have the same sizes. Undeformed chip sizes were described by four parameters, determined in Fig. 6, (enlarged part of Fig. 5b).

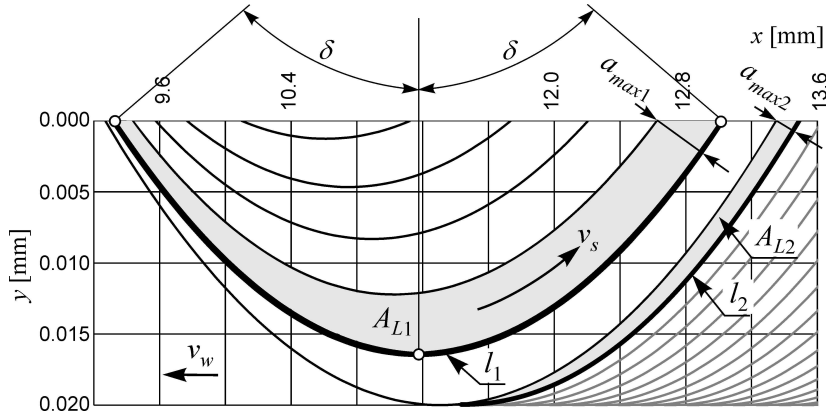


Fig. 6. Parameters of undeformed chip cut by grains in phase 1 and 2

The length l of undeformed chip is the total length of contact zone of the grain vertex with the work-material. The longitudinal cross-section area A_L of undeformed chip is limited by relative paths of successive grain vertices and flat nominal surface of material. The mean thickness a_m of undeformed chip is calculated as a ratio $A_L:l$ and maximal thickness a_{max} is the dimension perpendicular to grain path in exit (for up-grinding) or entrance (for down-grinding) point. In derivation of undeformed chip parameters, one takes advantage of the cycloid symmetry, and uses angle δ which depends on radius $\rho(\alpha)$:

$$\delta = \arccos\left(\frac{R-d}{\rho(\alpha)}\right) \Rightarrow \sin \delta = \sqrt{1 - \left[\frac{R-d}{\rho(\alpha)}\right]^2} \Rightarrow \delta \approx \sqrt{1 - \left[\frac{R-d}{\rho(\alpha)}\right]^2} \quad (13a, b, c)$$

Undeformed chip parameters for grains located in zone 1, for up- (UG) and down-grinding (GD), are as follows:

$$l_{1UG} = [\rho(\alpha) + r] 2\delta \approx 2[\rho(\alpha) + Rv^*] \sqrt{1 - \left[\frac{R-d}{\rho(\alpha)}\right]^2} \quad (14a)$$

$$l_{1DG} = [\rho(\alpha) - r] 2\delta \approx 2[\rho(\alpha) - Rv^*] \sqrt{1 - \left[\frac{R-d}{\rho(\alpha)}\right]^2} \quad (14b)$$

$$A_{L1UG} = \frac{d\rho(\alpha)}{d\alpha} \frac{l_g}{\rho^2(\alpha)} \left\{ [\rho^2(\alpha) + 2Rv^*(R-d)]\delta + [\rho(\alpha) + 2Rv^*][\rho(\alpha) - (R-d)] \frac{1}{\delta} \right\} \quad (15a)$$

$$A_{L1DG} = \frac{d\rho(\alpha)}{d\alpha} \frac{l_g}{\rho^2(\alpha)} \left\{ [\rho^2(\alpha) - 2Rv^*(R-d)]\delta + [\rho(\alpha) + 2Rv^*][\rho(\alpha) - (R-d)] \frac{1}{\delta} \right\} \quad (15b)$$

$$a_{\max 1UG} \approx \frac{fdl_g}{2\pi R} (1 + v^*) \operatorname{tg} |\kappa| \quad a_{\max 1DG} \approx \frac{fdl_g}{2\pi R} (1 - v^*) \operatorname{tg} |\kappa| \quad (16a, b)$$

Undeformed chip parameters for grains located in zone 1 are the same as for conventional grinding with a wheel without helical groove:

$$l_{2UG} \approx (1 + v^*) \left(\sqrt{2Rd - d^2} + v^* \frac{l_g}{2} \right) \quad (17a)$$

$$l_{2DG} \approx (1 - v^*) \left(\sqrt{2Rd - d^2} + v^* \frac{l_g}{2} \right) \quad (17b)$$

$$A_{L2UG} \approx l_g d v^* (1 + v^*) \quad A_{L2DG} \approx l_g d v^* (1 - v^*) \quad (18a, b)$$

$$a_{m2UG} = a_{m2DG} \approx \frac{rl_g d}{R \sqrt{2Rd - d^2}} \approx l_g v^* \sqrt{\frac{d}{2R}} \quad (19)$$

$$a_{\max 2UB} = a_{\max 2DB} = 2 \frac{v_w}{v_s} l_g \sqrt{\frac{d}{2R}} = 2a_{m2} \quad (20)$$

The differences between undeformed chip sizes for up- and down-grinding are usually neglected for small v^* ratios, applied to conventional grinding. The differences increase with growing v^* values, and for the presented method may exceed 10%. An example of the sizes of undeformed chip cut by abrasive grains from zone 1 and 2, calculated according to Eqs. (14–20), is shown in Fig. 7.

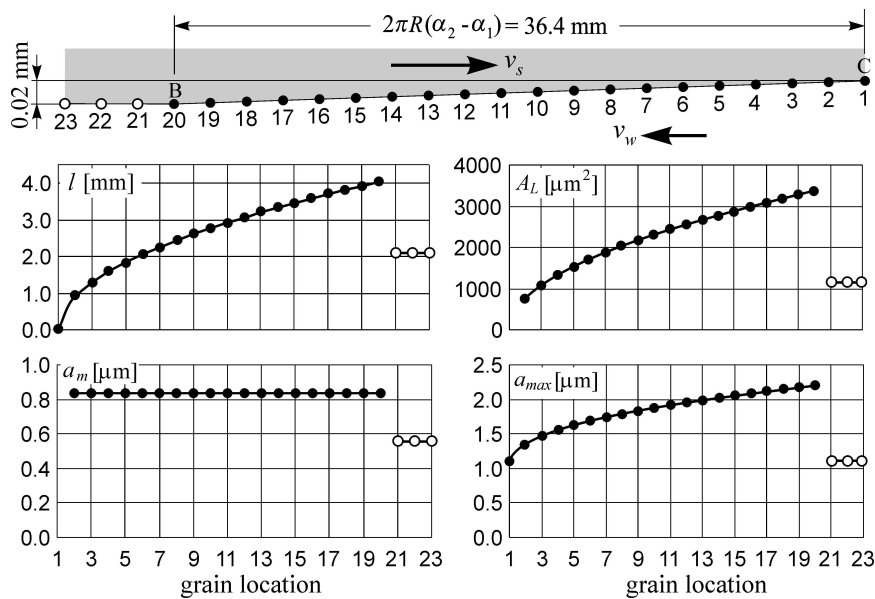


Fig. 7. Parameters of undeformed chips cut by grains located in zone 1 (black points) and 2 (white points) for up-grinding ($R = 100$ mm, $h = 0.04$ mm, $r_D = 2$ mm, $f_d = 2$ mm, $d = 0.02$ mm; $v^* = 0.0333$, $l_g = 1.666$ mm)

The analysis of grinding process with deterministic arrangement of grains shows that:

1. Among all active grains, most loaded are grains located at the boundary of zone 1 and 2. This fact suggests that these grains should wear intensively. If the wear mechanism consists in brittle bond or grain fracture, active edge of helical groove will systematically round off, grain load will be more uniform and hence wear process will decelerate. Such wear mechanism applies to soft wheels, as their bond bridges tend to crush. Hard wheels wear in a different way, and such a mechanism will not occur – wheel glazing is more typical wear mechanism and disadvantageous grinding burns may then occur.
2. Both wheel wear mechanisms (according to the first conclusion) do not cause (in long terms) any reduction of depth d of the grooves shaped on work-material, if the length c of cylindrical fragment of helical groove profile (Fig. 2a) remains greater than zero. Successive spalling of most loaded abrasive grains causes slow reduction of length c , which affects reduction of groove bottoms b , groove lengths l_r and increases the length l_b of flat bearing segments.

5. Undeformed chip sizes – probabilistic model

Probabilistic model of the wheel assumes that grain vertices are arranged randomly, both in circumferential and radial directions. Main problem with modelling random distribution of abrasive grains is to determine the expected number of grain vertices at the wheel circumference. Measurements of the number C_A of cutting edges observed on the wheel surface unit make it possible to calculate mean distance l_g between cutting edges in any direction:

$$l_g = \frac{1}{\sqrt{C_A}} \quad (21)$$

However, modelling the grinding process, in the plane perpendicular to wheel axis, one needs to know the mean directional distance \bar{l}_g between adjacent cutting edges in the specific plane, which is clearly greater than l_g . The distance \bar{l}_g was determined according to the scheme from Fig. 8.

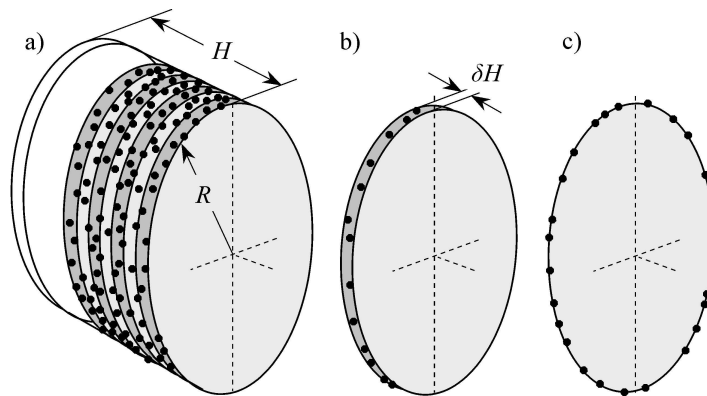


Fig. 8. Scheme of wheel segmentation into elementary slices of width δH (b), reduced to single plane (c)

The expected number of grain vertices distributed on entire wheel active surface (Fig. 8a) is equal to $E(w) = 2\pi RHC_A$, and depends on wheel radius R and wheel height H . The wheel is divided (Fig. 8b) into the so-called elementary slices of heights $\delta H \ll H$ close to the dimensions of interaction zone between single grain and work-material. The expected number of grain vertices located at the circumference of single elementary slice is $E(s) = 2\pi R\delta HC_A$. The mean directional distance \bar{l}_g between adjacent grain vertices is the ratio between entire length $2\pi R$ of circumference and the expected number $E(s)$ of grain vertices:

$$\bar{l}_g = \frac{1}{\delta HC_A} \quad (22)$$

It is assumed that the directional distance \bar{l}_g between adjacent grain vertices is the same for the whole analysed plane (Fig. 8c), as δH is small enough. An example based on the data for the wheel 98A-60-K-6-V ($C_A = 6 \text{ mm}^{-2}$) [42] confirms that the mean distance $l_g = 0.408 \text{ mm}$, calculated by using Eq. (21) is clearly smaller than the mean directional distance $\bar{l}_g = 1.6(6) \text{ mm}$, calculated for $\delta H = 0.1 \text{ mm}$ by using Eq. (22).

Circumferential distribution of grains is uniform. It means that the probability density function of incremental angles $\Delta\alpha_i$ between adjacent grain vertices is exponential. To generate sequential values $\Delta\alpha_i$, one uses equation (23) resulting from converse transformation of cumulative distribution function:

$$\Delta\alpha_i = -\frac{\bar{l}_g}{R} \ln [1 - Rnd] \quad (23)$$

where Rnd is a random number generated from the range (0; 1). Procedure (23) is repeated n times until $\Sigma\Delta\alpha_i \geq 2\pi$, so that the number n of grain vertices is a random variable.

Radial coordinates of grains are equal to the local radius $\rho(\alpha)$ decreased by random deviation $\Delta\rho_i$. The $\Delta\rho_i$ values are described by Weibull distribution as it is well-founded [44], [45] and confirmed experimentally [46]. Cumulative Weibull distribution function, determined by the shape parameter $m > 0$ [-] and scale parameter $u > 0$ [mm], has converse transformation. It allows one to generate radial deviations $\Delta\rho_i$, by using random number Rnd generator, according to the following equation:

$$\Delta\rho_i = -u \sqrt[m]{\ln(1 - Rnd)} \quad (24)$$

An example of random arrangement of grain vertices, generated in the plane perpendicular to wheel axis, is shown in Fig. 9. In this example, from among the total number $n = 387$ of grain vertices generated, only $n_{PA} = 236$ potential active vertices are located at radiuses $\rho(\alpha) \geq R - d$. Inactive grain vertices, located at radiuses $\rho(\alpha) < R - d$ and marked with grey colour, cannot be in contact with the work-material.

Relation $\rho(\alpha) \geq R - d$ is not a sufficient condition for grain activity, as the grain can move along a path which does not cross the work-material surface shaped by previous active grains. As the distance $\Delta\alpha$ and the radius $\rho(\alpha)$ increase, the probability of grain activity also increases. Both factors may be integrated into one sufficient condition, based on the relation between abscissas x_{ex} , of exit points, calculated (Eq. 7a) for each potential active grain. If x_{exn} (for a given potential active vertex) is greater (for up-grinding) than x_{exp} pertaining to the previous active vertex, then this vertex is active. Such a condition applies to both cases: when successive paths do not cross

(Fig. 10a) or cross (Fig. 10b, c), irrespective of relation between radiuses of analysed pair of grains.

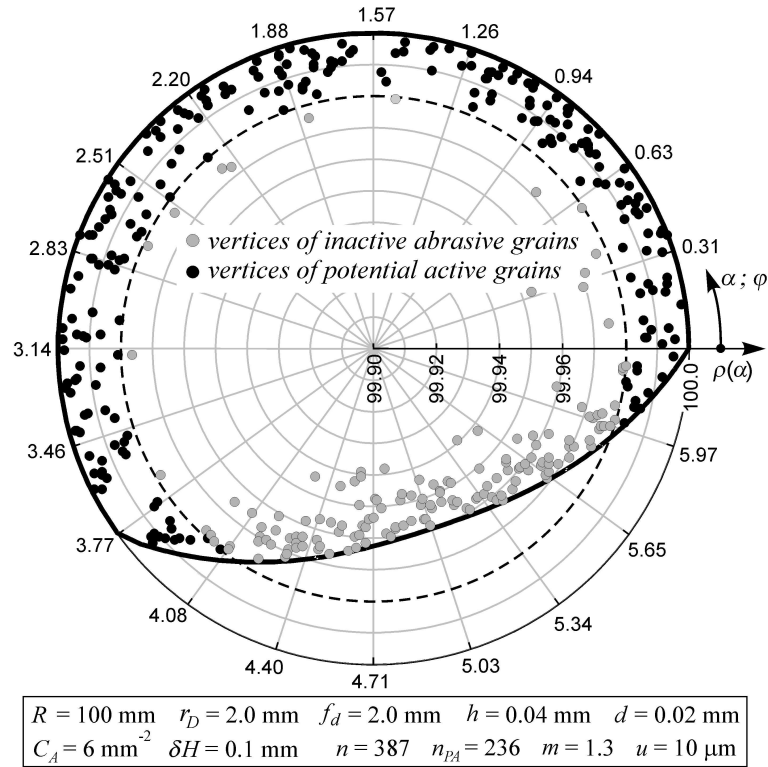


Fig. 9. An example of random arrangement of grain vertices in the plane perpendicular to wheel axis

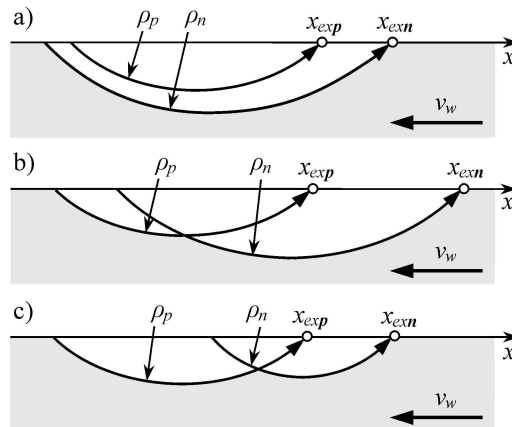


Fig. 10. Three possible situations of activity of the next possibly active grain – subscript “p” denotes previous possibly active grain and subscript “n” denotes next possibly active grain [10]

As the result of identification of active vertices, active vertices were found for the wheel shown in Fig. 9, $n_A = 83$ as 21% of entire n vertices, and 35% of n_{PA} potential active vertices. Relative path were calculated for each active vertex, according to Eq. (6a), as it was shown in Fig. 11a for one wheel rotation.

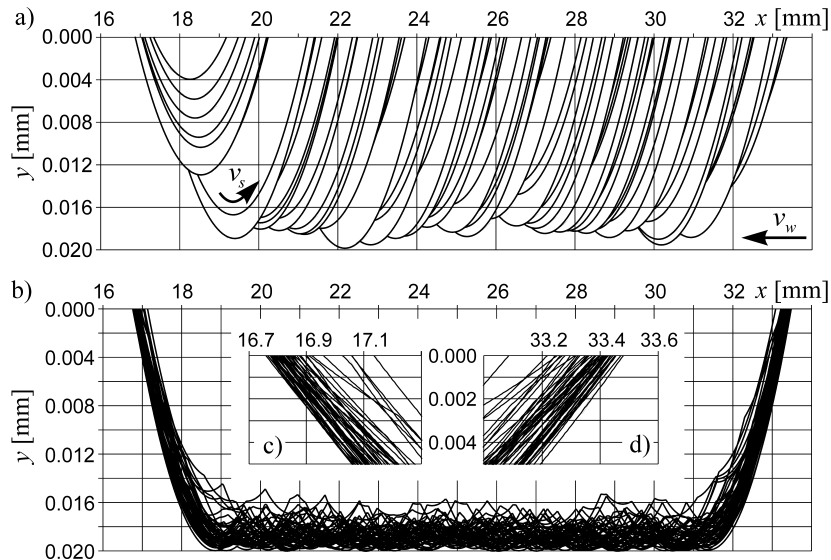


Fig. 11. Paths (a) of $n_A = 83$ active vertices, located on wheel circumference, as in Fig. 9, for up-grinding with $v^* = 0.0333$ and 50 profiles (b, c, d) of grooves shaped on the work-material by wheels with different grain arrangements [10]

Longitudinal profile of the groove shaped on the work-material is not as regular as the profile obtained with deterministic model (Fig. 5), and it manifests by rough bottom of the groove and different shapes of slopes. Non-uniform load of grains located in zone 2 is also visible. Because of random arrangement of abrasive grains, some of grains located in zone 3 are active.

The conclusions following on one simulation should not be generalized as each simulation has only the meaning of a single element from a random sample. More general conclusions could be obtained by multiple repetition of the simulation procedure. Fig. 11b shows longitudinal profiles of 50 grooves obtained for the same input data, in which the coordinates $\rho(\alpha)$ of grain vertices have been differentiated. Individual groove profiles differ from each other, but the results of wheel reproduction are very similar. Dimensions of the grooves differ slightly, and it is visible in Figs. 11c, d that illustrates both ends of 50 grooves.

Undeformed chip sizes were determined similarly to deterministic model, by comparison of successive grain paths. Four parameters (l, A_L, a_m, a_{max}) of undeformed chip sizes were calculated for each active vertex, as shown

in Figs. 9 and 11. Procedure was repeated 50 times, giving the total number of $n_A = 4116$ undeformed chips shown in Fig. 12. The percentage of active grain vertices, located in zones 1, 2, and 3, were 8.84%, 89.3% and 1.8% of all active vertices, respectively.

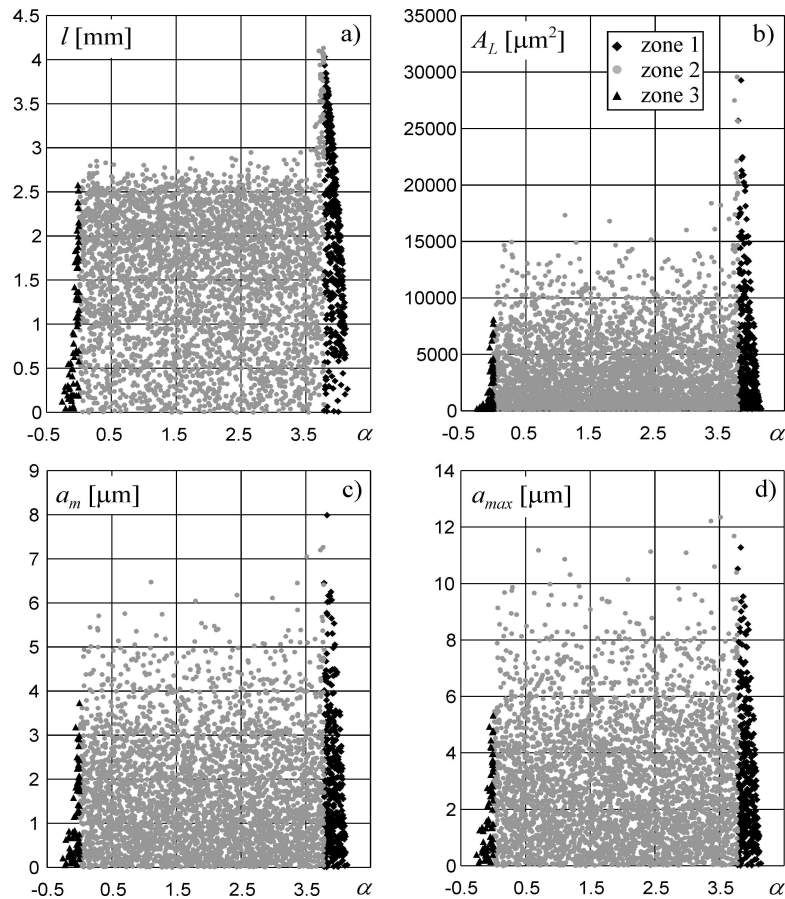


Fig. 12. Undeformed chip parameters vs. grains angular position for $n_A = 4116$ active grains identified in 50 repetition of simulation procedure for up-grinding ($v^* = 0.0333$) for input data according to Fig. 9 [10]

As it has been supposed, every parameter (l , A_L , a_m , a_{max}) of undeformed chips shows a serious dispersion. Simulation results confirm that the most loaded abrasive grains are located in zones 1 and 2; the boundary – cross-section areas A_L (Fig. 12b) show it most clearly. Cross-section areas A_L from Fig. 12b are plotted vs. α in Fig. 13. The square regression of A_L vs. α , determined for grains located in zone 1 and the linear regression, determined for grains located in zone 2, show characteristic discontinuity at the boundary of zones 1 and 2 predicted by the deterministic model (see Fig. 7).

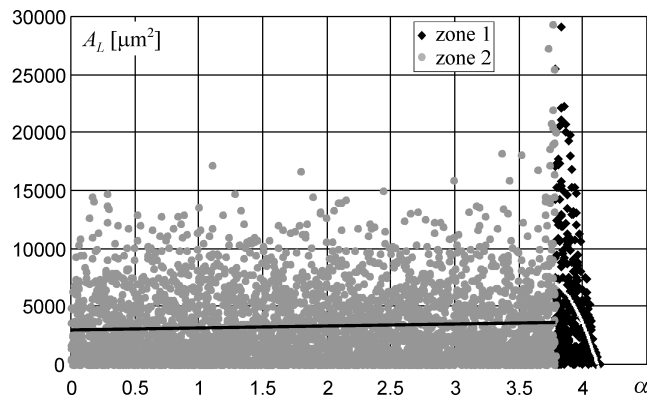


Fig. 13. Characteristics of regressions between undeformed chip cross-section areas A_L and circumferential location of grain vertices determined by angle α for zone 1 (white line) and zone 2 (black line) for input data according to Fig. 9

The histograms from Fig. 14 show distribution of undeformed chip parameters (l , A_L , a_m , a_{max}). Distribution of A_L is similar to an exponential one, while other distributions are more complex and cannot be represented by typical probability distributions.

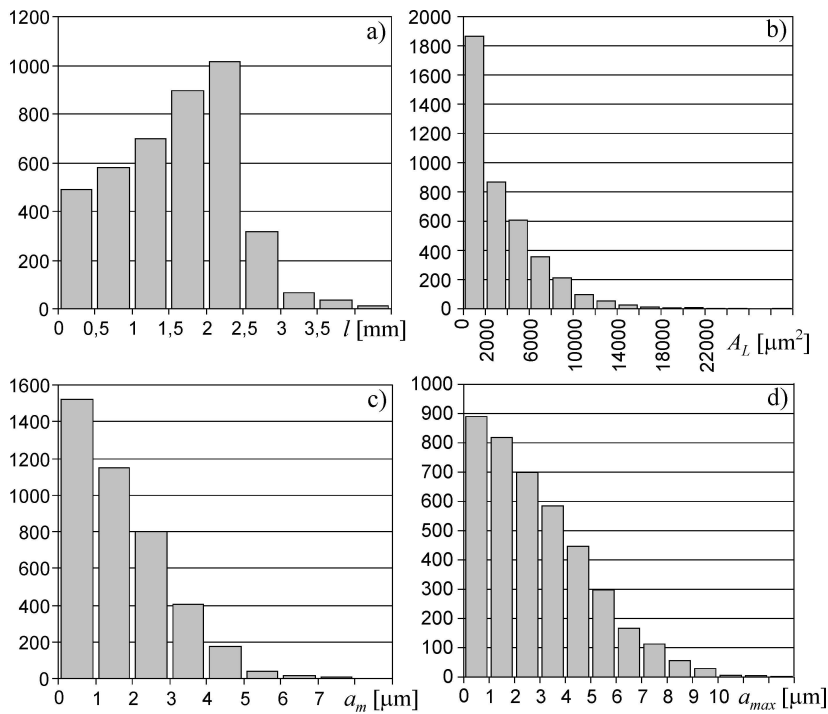


Fig. 14. Histograms of length (a), cross-section area (b), mean thickness (c) and maximal thickness (d) of $n_A = 4116$ undeformed chips obtained in simulation procedure, repeated 50 times for input data according to Fig. 9 [10]

Table 2.

Input data sets differing from baseline set (#1) by one input variable (grey areas)

Input data number	f_d [mm]	h [mm]	r_D [mm]	\bar{l}_g [mm]	m [-]	u [mm]	d [mm]	v^* [-]
1 (baseline)	2	0.04	2	1.667	1.3	0.01	0.02	0.033
2	1	0.04	2	1.667	1.3	0.01	0.02	0.033
3	3	0.04	2	1.667	1.3	0.01	0.02	0.033
4	2	0.02	2	1.667	1.3	0.01	0.02	0.033
5	2	0.06	2	1.667	1.3	0.01	0.02	0.033
6	2	0.04	1	1.667	1.3	0.01	0.02	0.033
7	2	0.04	3	1.667	1.3	0.01	0.02	0.033
8	2	0.04	2	3.333	1.3	0.01	0.02	0.033
9	2	0.04	2	0.833	1.3	0.01	0.02	0.033
10	2	0.04	2	1.667	1	0.01	0.02	0.033
11	2	0.04	2	1.667	1.6	0.01	0.02	0.033
12	2	0.04	2	1.667	1.3	0.005	0.02	0.033
13	2	0.04	2	1.667	1.3	0.015	0.02	0.033
14	2	0.04	2	1.667	1.3	0.01	0.01	0.033
15	2	0.04	2	1.667	1.3	0.01	0.03	0.033
16	2	0.04	2	1.667	1.3	0.01	0.02	0.067
17	2	0.04	2	1.667	1.3	0.01	0.02	0.011

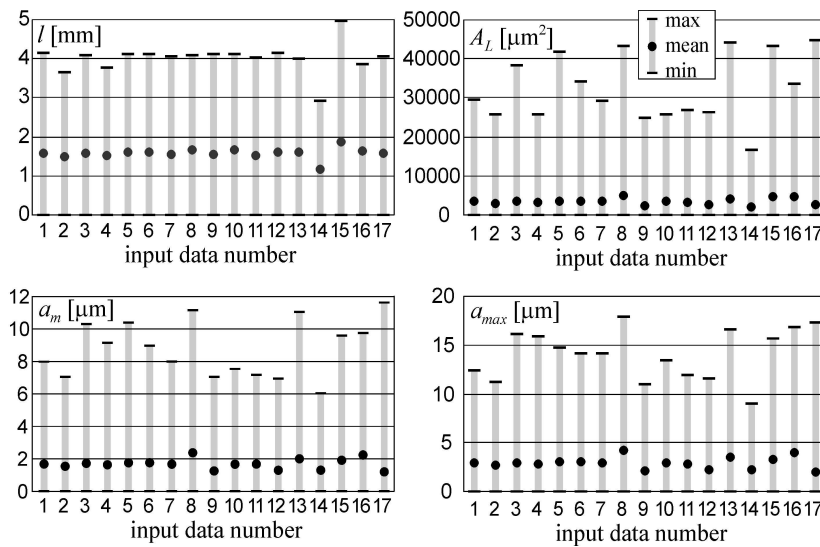


Fig. 15. Ranges of undeformed chip parameters for 17 sets of input data (Table 2) obtained in simulation procedure repeated 50 times

Neither the effect of wheel parameters (f_d , h , r_D , \bar{l}_g , m , u), nor that of grinding parameters (d , v^*) are shown by the probabilistic model as clearly as by the deterministic model. To find the effect of eight input variables on the result of the process, 50 simulations were performed for each of 17 sets

of input data differentiated with respect to the baseline set by only one input variable (Tab. 2). The entire result consist of great numbers $\Sigma n = 329106$, $\Sigma n_{PA} = 196342$ and $\Sigma n_A = 69211$ of generated, potential active and active grain vertices, respectively. The results obtained for baseline input data (#1) have been presented above. The comparison of results obtained for all 17 sets of input data is shown in Fig. 15.

Wide ranges of undeformed chip sizes are evident – standard deviation to mean value ratios are equal 53%, 107%, 77% and 75%, for l , A_L , a_m , a_{max} , respectively. The effect of individual input variable can be found by comparison of results of three sets of input data, including the baseline set. For instance, comparison of undeformed chip sizes for input data sets numbered as 1, 2 and 3 shows the effect of helical groove pitch f_d , while comparison of sets 1, 14 and 15 shows the effect of grinding depth d .

It is interesting to compare the quantitative results of both models. Mean value of longitudinal cross-section area A_L , shown in Figs. 12b and 13 for grains located in zone 2, is equal to $3288 \mu\text{m}^2$, i.e. almost three times greater than $A_{L2} = 1148 \mu\text{m}^2$, calculated for the same data according to Eq. (18a), (see Fig. 7). The difference can be easily explained, as all grains in the deterministic model are active, while only one third (35%) of grains generated on the wheel circumference are active in the probabilistic model. Lower number of active grains means that each active grain removes three times greater volume of material than that removed by grains arranged in regular way and located at the same radiuses.

6. Conclusions

1. Deterministic model of the wheel, assuming uniform and regular arrangement of grains provides very simplified wheel representation. However, such model gives satisfactory description of mechanism of wheel reproduction and allows one to evaluate the effects of an individual input variable on the process results. Deterministic model is especially useful for the choice of parameters, providing required RTS of work-material.
2. Deterministic approach clearly shows qualitative effects of an individual input variable on parameters of undeformed chips. Quantitative description is not precise enough, because of assumptions used in the model.
3. Probabilistic approach, assuming random arrangement of grain vertices in both radial and circumferential directions, shows that the values of parameters of undeformed chips are strongly randomised – their standard deviations are comparable to the mean values. Random arrangement of grains strongly affects parameters of undeformed chips and roughness of groove bottoms.

4. Mean values of the thickness and cross-section areas of undeformed chips, obtained with the probabilistic model, are clearly greater than values resulting from deterministic model. The difference arises from different activity ratio of abrasive grains, which is many times lower for grains arranged in a random way. Hence, the entire excess material is removed by a smaller number of active grains.
5. The most loaded abrasive grains are located at the boundary between zone 1 and 2. Random arrangement of grains may cause that grains located in zone 3 are also active, but they participate in material removal to a minimal extent.
6. The main output quantities of the process are dimensions, shape and arrangement of grooves formed on the work-material. Dimensions of individual grooves should be formally described as random variables, but they do not differ significantly from nominal dimensions yielded by deterministic approach. Standard deviations to mean value ratios of groove dimensions do not exceed 1%. The reproduction mechanism is hence much more deterministic than stochastic, although grains are arranged in a random way. The influence of random arrangement of abrasive grains on the dimensions and arrangements of the grooves is minimal.

Manuscript received by Editorial Board, November 07, 2006;
final version, May 15, 2007.

REFERENCES

- [1] Ocoś K., Liubimov V.: *Struktura geometryczna powierzchni. Podstawy klasyfikacji z atlasem charakterystycznych powierzchni kształtowanych*. Oficyna Wydawnicza Politechniki Rzeszowskiej, Rzeszów 2003.
- [2] Stout K. J., Blunt L.: A contribution to the debate on surface classifications - random, systematic, unstructured, structured and engineered. *International Journal of Machine Tools and Manufacture*, 2001, Vol. 41, pp. 2039÷2044.
- [3] Stępień P.: Właściwości eksploatacyjne powierzchni o regularnej makrogeometrii. *Zeszyty Naukowe Politechniki Rzeszowskiej*, 1987, Nr 35, z. 14, XV Szkoła Trybologiczna, Rzeszów, pp. 123÷125.
- [4] Stępień P.: *Oberflächengestaltung gasdynamischer Lager und Dichtungen*. *Industrie Diamanten Rundschau*, 1994, Vol. 2, pp. 108÷114.
- [5] Bulatov V. P., Krasny V. A., Schneider Y. G.: Basic of machining methods to yield wear- and fretting-resistive surfaces, having roughness patterns. *Wear*, 1997, Vol. 208, pp. 132÷137.
- [6] Kobatake S., Kawakubo Y., Suzuki S.: Laplace pressure measurement on laser textured thin-film disk. *Tribology International*, 2003, Vol. 36, pp. 329÷333.
- [7] Wakuda M., Yamauchi Y., Kanzaki S., Yasuda Y.: Effect of surface texturing on friction reduction between ceramic and steel materials under lubricated sliding contact. *Wear*, 2003, Vol. 254, pp. 356÷363.

- [8] Kovalchenko A., Ajayi O., Erdemir A., Fenske G., Etsion I.: The effect of laser surface texturing on transitions in lubrication regimes during unidirectional sliding contact. *Tribology International*, 2005, Vol. 38, pp. 219÷225.
- [9] Pettersson U., Jacobson S.: Tribological texturing of steel surfaces with a novel diamond embossing tool technique. *Tribology International*, 2006, Vol. 39, pp. 695÷700.
- [10] Stępień P.: Podstawy kształtowania regularnej struktury geometrycznej powierzchni w procesach szlifowania. Wydawnictwo Uczelniane Politechniki Koszalińskiej, Monografia Nr 125, Koszalin 2006.
- [11] Gao W., Araki T., Kiyono S., Okazaki Y., Yamanaka M.: Precision nanofabrication and evaluation of a large area sinusoidal grid surface for a surface encoder. *Precision Engineering*, 2003, Vol. 27, pp. 289÷298.
- [12] Ike H.: Properties of metal sheets with 3-D designed surface microgeometry prepared by special rolls. *Journal of Materials Processing Technology*, 1996, Vol. 60, pp. 363÷368.
- [13] Ike H., Plancak M.: Coining process as a means of controlling surface microgeometry. *Journal of Materials Processing Technology*, 1998, Vol. 80–81, pp. 101÷107.
- [14] Forniés E., Zaldo C., Albella J. M.: Control of random texture of monocrystalline silicon cells by angle-resolved optical reflectance. *Solar Energy Materials and Solar Cells*, 2005, Vol. 87, pp. 583÷593.
- [15] Xi Z., Yang D., Que D.: Texturization of monocrystalline silicon with tribasic-sodium phosphate. *Solar Energy Materials and Solar Cells*, 2003, Vol. 77, pp. 255÷263.
- [16] Schneider Y.G.: Formation of surface with uniform micropatterns on precision machine and instrument parts. *Precision Engineering*, 1984, Vol. 6(14), pp. 219÷225.
- [17] Arola D., McCain M. L., Kunaporn S., Ramulu M.: Waterjet and abrasive waterjet surface treatment of titanium: a comparison of surface texture and residual stress. *Wear*, 2002, Vol. 249, pp. 943÷950.
- [18] Ramasawmy H., Blunt L.: Effect of EDM process parameters on 3D surface topography. *Journal of Materials Processing Technology*, 2004, Vol. 148, pp. 155÷164.
- [19] Choo L., Ogawa Y., Kanbargi G., Otrá V., Raff L. M., Komanduri R.: Micromachining of silicon by short-pulse laser ablation in air and under water. *Materials Science and Engineering*, 2004, Vol. A372, pp. 145÷162.
- [20] Du D., He Y. F., Sui B., Xiong L. J., Zhang H.: Laser texturing of rollers by pulsed Nd:YAG laser. *Journal of Materials Processing Technology*, 2005, Vol. 161, pp. 456÷461.
- [21] Hong M. H., Huang S. M., Luk'yanchuk B. S., Chong T. C.: Laser assisted surface nanopatterning. *Sensors and Actuators*, 2003, Vol. A108, pp. 69÷74.
- [22] Horisawa H., Akimoto N., Ashizawa H., Yasunaga N.: Effects of a quartz beam-guide on high-precision laser-assisted etching of Al₂O₃ ceramics. *Surface and Coatings Technology*, 1999, Vol. 112, pp. 389÷393.
- [23] Lee Y.-C., Chen C.-M., Wu C.-Y.: A new excimer laser micromachining method for axially symmetric 3D microstructures with continuous surface profiles. *Sensors and Actuators*, 2005, Vol. A117, pp. 349÷355.
- [24] Man H. C., Zhang S., Cheng F. T., Guo X.: Laser fabrication of porous surface layer on NiTi shape memory alloy. *Materials Science and Engineering*, 2005, Vol. A404, pp. 173÷178.
- [25] Tsai C.-H., Chen H.-C.: Laser milling of cavity in ceramic substrate by fracture-machining element technique. *Journal of Materials Processing Technology*, 2003, Vol. 136, pp. 158÷165.
- [26] Yakimets I., Richard C., Béranger G., Peyre P.: Laser peening processing effect on mechanical and tribological properties of rolling steel 100Cr6. *Wear*, 2004, Vol. 256, pp. 311÷320.
- [27] Stępień P.: Sposób nacinania regularnych rowków na powierzchni przedmiotu oraz narzędzie do nacinania regularnych rowków na powierzchni przedmiotu. Patent 137408 z 03.03.1988.
- [28] Kacalak W., Pluta Z., Stępień P.: Nowe metody i narzędzia do kształtowania regularnej makrogeometrii na powierzchniach utwardzonych. *Prace naukowe ITBM Politechniki Wrocławskiej*, 1987, Nr 34, X Naukowa Szkoła Obróbki Ściernej, pp. 227÷236.

- [29] Stępień P.: Nowa metoda nacinania regularnych rowków na powierzchniach części maszyn. Materiały II Krajowej Konferencji Naukowo-Technicznej „Nowoczesne technologie w budowie maszyn ciężkich”, 1987, pp. 136÷147.
- [30] Stępień P.: Nowa metoda kształtowania regularnej makrogeometrii powierzchni technicznych. Zeszyty Naukowe Politechniki Rzeszowskiej Nr 36, z. 14, XV Szkoła Trybologiczna, 1987, pp. 123÷125.
- [31] Stępień P.: Analiza hydrodynamicznego wyporu mikroklinów smarnych. Zeszyty Naukowe Politechniki Rzeszowskiej Nr 36, z. 14, XV Szkoła Trybologiczna, 1987, pp. 231÷236.
- [32] Stępień P.: Analiza obciążenia ziaren przy szlifowaniu ściernicą kształtującą regularną strukturę geometryczną powierzchni technicznych. Materiały II Konferencji „Narzędzia Skrawające i ściernie NASS '88”, 1988, pp. 317÷325.
- [33] Kacalak W., Stępień P.: Metody kształtowania ściernego regularnej makrogeometrii na powierzchniach utwardzonych. Materiały II Międzynarodowego Sympozjum „Obróbka dokładna i wykończająca – FPM '89”, 1989, Prace Naukowe ITBM Politechniki Wrocławskiej Nr 42, Seria: Konferencje Nr 15, pp. 24÷33.
- [34] Stępień P.: Generation of regular patterns on ground surfaces. Annals of the CIRP, 1989, Vol. 38/1, pp. 561÷566.
- [35] Stępień P., Bałasz B.: Simulation of the formation process of regular grooves on the ground surface. Proc. 4th Annual Industrial Simulation Conference, Palermo 5–6 June 2006, 269÷276.
- [36] Stępień P.: Sposób nacinania regularnych rowków na powierzchni przedmiotu obrotowego. Patent 160313 z 21.01.1994.
- [37] Gołąbczak A.: Metody kształtowania właściwości użytkowych ściernic. Monografie, Politechnika Łódzka, 2004.
- [38] Gołąbczak A.: System elektroerozyjnego i elektrochemicznego obciążania ściernic ze spoiwem metalowym. Szkoła Naukowa Obróbek Erozyjnych, 2000, Vol. 7, pp. 141÷154.
- [39] Yokogawa K.: Einfluß der Abricht- und Schleifbedingungen auf die Rauheit und Rundheit geschliffener Oberflächen. Werkstatt und Betrieb, 1974, Vol. 9, pp. 513÷588.
- [40] Verkerk J., Pekelharing A. J.: Kinematical approach to the effect of wheel dressing conditions on the grinding process. Annals of the CIRP, 1976, Vol. 25/1, pp. 209÷214.
- [41] Verkerk J., Pekelharing A. J.: The influence of the dressing operation on productivity in precision grinding. Annals of the CIRP, 1979, Vol. 28/2, pp. 487÷495.
- [42] Verkerk J.: Final report concerning CIRP cooperative work on the characterization of grinding wheel topography. Annals of the CIRP, 1976, Vol. 25/1, pp. 209÷215.
- [43] Renker H. J.: The identification of grinding faults from appearance of ground surface. Technical Information STUDER AG, 1981, Vol. 10, pp. 1÷12.
- [44] Stępień P.: Wybrane zagadnienia procesu kształtowania topografii powierzchni szlifowanej. Praca Doktorska, Wrocław 1984.
- [45] Stępień P.: Rozmieszczenie wierzchołków ziaren ściernych na roboczej powierzchni ściernicy. Zeszyty Naukowe Wydziału Mechanicznego Wyższej Szkoły Inżynierskiej w Koszalinie, 1989, Nr 11, pp. 233÷252.
- [46] Stępień P.: Badania topografii powierzchni ściernic z regularnego azotku boru. Materiały XIX Naukowej Szkoły Obróbki Ścierniej, 1996, pp. 131÷137.

Rozmiary warstw skrawanych w procesie szlifowania regularnej struktury geometrycznej powierzchni**S t r e s z c z e n i e**

Praca przedstawia analizę teoretyczną i wyniki badań symulacyjnych procesu kształtowania regularnej struktury geometrycznej powierzchni przy szlifowaniu specjalnie ukształtowaną ściernicą z pojedynczym rowkiem śrubowym. Opisano nierównomierne obciążenie ziaren ściernych położonych na różnych częściach obwodu ściernicy. Zastosowano dwa modele czynnej powierzchni ściernicy, różniące się sposobem rozmieszczenia ziaren ściernych. Wyniki obu modeli: deterministycznego oraz probabilistycznego zostały porównane, a istniejące różnice wyjaśnione.